Case Studies in Construction Materials 24 (2026) e05893

Contents lists available at ScienceDirect

Case Studies in Construction Materials

journal homepage: www.elsevier.com/locate/cscm

Mechanical degradation of naturally corroded rebars from a 45-year-old bridge slab: 3D quantification of section loss and a new corrosion damage indicator

Jihun Shin [a], Chang-Su Shim [b,*]

[a] Department of Smart Cities, Chung-Ang University, Seoul 06974, Republic of Korea
[b] Department of Civil and Environmental Engineering, Chung-Ang University, Seoul 06974, Republic of Korea

ARTICLE INFO

Keywords:
Naturally corroded reinforcing bars
Bridge slab
3D surface reconstruction
Corrosion damage indicator
Residual tensile strength
Empirical corrosion model

ABSTRACT

Corrosion of reinforcing steel is a principal cause of degradation and strength loss in reinforced concrete (RC) structures, particularly those exposed to aggressive environmental conditions over extended service periods. This study investigates the residual mechanical performance of fifty-seven naturally corroded rebars extracted from a 45-year-old bridge deck. Based on chloride exposure records and damage inspection, corrosion initiation was estimated to have occurred approximately 24 years after construction. A simplified three-dimensional reconstruction method was developed to capture local cross-sectional loss and pit depth at the fracture zone. The resulting geometric indicators were then correlated with the tensile properties—yield strength, ultimate strength, and elongation—to assess the mechanical degradation due to corrosion. Among the tested parameters, a combined index incorporating maximum pit depth and residual cross-sectional area exhibited the strongest and most consistent correlation with mechanical strength, effectively reducing the data scatter typical of single-parameter models. The proposed empirical relationships provide a practical approach for estimating the residual tensile capacity of corroded reinforcement, thereby supporting quantitative durability assessment and service-life prediction of long-term RC bridge structures.

1. Introduction

Among the members of a bridge superstructure, the slab is particularly susceptible to deterioration due to its direct exposure to vehicular loads and environmental conditions. Over time, it degrades through mechanisms such as cracking, chloride penetration, and carbonation, which collectively accelerate rebar corrosion [1,2]. The reinforcing bars, which serve as the main material responsible for resisting tensile forces in RC bridge deck slabs, experience non-uniform cross-sectional loss due to corrosion, leading to a progressive decline in mechanical performance and, in severe cases, potential structural collapse [3].

In the current maintenance process of aging bridge slabs, repair and reinforcement are conducted by measuring the degree of corrosion in the reinforcing bars after removing the concrete cover using a water jet. However, to accurately predict the remaining service life and performance degradation of the structure, a quantitative and reliable material-level experimental study based on data obtained from specimens extracted from actual structures is essential [4].

* Corresponding author.
E-mail addresses: jihunshin@cau.ac.kr (J. Shin), csshim@cau.ac.kr (C.-S. Shim).

https://doi.org/10.1016/j.cscm.2026.e05893
Received 11 November 2025; Received in revised form 27 January 2026; Accepted 12 February 2026
Available online 13 February 2026
2214-5095/© 2026 The Authors. Published by Elsevier Ltd. This is an open access article under the CC BY-NC-ND license (http://creativecommons.org/licenses/by-nc-nd/4.0/).

Therefore, this study proposes a practical empirical model that quantifies the degree of corrosion and predicts the mechanical degradation of rebars, thereby enhancing the reliability of maintenance decision-making. Previous studies on rebar corrosion have typically formulated empirical equations using the mass loss ratio or average cross-sectional loss as representative corrosion indicators, while others have introduced the maximum cross-sectional loss and maximum pit depth as alternative parameters [3,5,6]. However, these single indicators alone are insufficient to capture the stress concentration effects of non-uniform corrosion, leading to reduced reliability and increased prediction scatter when applied to the maintenance of actual structures [4,7,8].

Against this background, numerous experimental studies have been conducted to investigate the degradation in the mechanical performance of corroded rebars. However, obtaining naturally corroded specimens from in-service structures remains challenging. Therefore, to reproduce corroded rebars, research has been actively conducted using artificial corrosion techniques, such as electrochemical corrosion and salt-spray tests [6]. Nevertheless, corrosion in real structures occurs not only through chloride attack, carbonation, and cracking but is also influenced by various factors such as concrete cover thickness, heavy traffic loading, and exposure conditions. Consequently, the results of artificial corrosion tests alone cannot fully represent the complex behavior observed in actual structures [4]. Therefore, this study conducted an empirical analysis using naturally corroded rebar specimens extracted from a 45-year-old bridge in service.

A total of 57 naturally corroded rebar specimens were quantitatively analyzed to determine the mass loss ratio, maximum pit depth, and corrosion length. The cross-sectional loss was further quantified using an image-based three-dimensional (3D) reconstruction technique [9]. Tensile tests were subsequently performed under displacement control at a loading rate of 8 mm/min to measure the yield and ultimate strengths of each specimen. Based on the quantified data, an empirical formula was presented to predict the mechanical performance of naturally corroded rebars by analyzing and comparing both single and combined corrosion indicators.

Accordingly, this study focuses on three main aspects. First, an empirical dataset of naturally corroded rebars was established using samples extracted from the deck slab of a 45-year-old bridge in service. Second, an image-based 3D reconstruction and automated cross-sectional slicing pipeline was developed to characterize corroded rebar geometry. Finally, a data-driven empirical model incorporating a composite corrosion indicator is introduced to address the limitations of conventional single-indicator empirical models.

2. Background on corrosion mechanisms and mechanical degradation of reinforcing bars

This section provides the technical background on reinforcement material characteristics, corrosion mechanisms, and corrosion-induced mechanical degradation of reinforcing bars. The reviewed studies establish the scientific basis for the corrosion indicators and experimental approaches adopted in the present work.

2.1. Type of reinforcing bar

The reinforcing bars used in the 45-year-old bridge were classified as SD300, a conventional hot-rolled deformed steel bar with a nominal yield strength of 300 MPa. According to the manufacturing standards of domestic steel producers such as HANSCO [10], rebars of grade SD400 and higher are generally produced through the Tempcore process, which involves rapid surface quenching to form a martensitic layer. This hardened layer, created when the cooling rate exceeds approximately 20–30 °C/s, improves both the mechanical performance and corrosion resistance of the bar due to its dense microstructure [11].

In contrast, SD300 rebars are manufactured without the Tempcore treatment and therefore lack a martensitic layer. Instead, they exhibit a uniform pearlitic microstructure throughout the cross-section [12]. In this study, the microstructural effects of layering were considered negligible, and all analyses were conducted under the assumption of a homogeneous steel composition.

2.2. Corrosion and mechanical degradation of reinforcing bars

Corrosion of reinforcing bars is one of the main deterioration mechanisms that directly influences the service life and structural safety of reinforced concrete (RC) bridges. Two primary forms are typically observed: uniform corrosion induced by carbonation and pitting corrosion triggered by chloride ingress [1]. Carbonation lowers concrete alkalinity by converting calcium hydroxide into calcium carbonate, leading to steel depassivation once the carbonation front reaches the rebar. In contrast, chloride-induced corrosion results in localized attack characterized by deep pits and non-uniform section loss. Such deterioration reduces the mechanical strength

Table 1
Summary of corrosion-induced mechanical degradation models for reinforcing steel.

Reference	Indicator	Yield Strength	Ultimate Strength	Ultimate Strain
[5]	C: Mass Loss D: Diameter	$f_y = 581.22 - 3.53C + 1.82D$	$f_s = 651.82 - 3.49C + 0.44D$	-
[6]	X: Mass Loss	$f_y = 1 - 0.0127x$	$f_s = 1 - 0.0116x$	$\varepsilon_{us} = 1 - 0.0281x$
[6]	X: Mass Loss	$f_y = 1 - 0.0123x$	$f_s = 1 - 0.115x$	$\varepsilon_{us} = 1 - 0.0125x$
[3]	*Mcorr* : Mass Loss	$f_y = 1 - 0.019961Mcorr$	$f_s = 1 - 0.18642Mcorr$	$\varepsilon_{us} = e^{-0.0546993Mcorr}$

and ductility of reinforcing bars and can ultimately compromise the structural integrity of RC members.

2.2.1. Corrosion rate indicators

Numerous studies have attempted to quantify the degradation of corroded rebars using various corrosion indicators, including mass loss ratio, average cross-sectional loss, and maximum pit depth [3,5,6,13–15]. Most empirical models relate the mass loss ratio to reductions in yield strength, ultimate strength, and ductility. For instance, Imperatore et al. [3] proposed empirical relationships linking mass loss to decreases in these mechanical parameters under both uniform and pitting corrosion conditions. Table 1 summarizes representative models reported in previous research.

Overall, the reviewed studies indicate that the strength of corroded rebars generally decreases linearly with increasing mass loss, whereas ductility tends to decline exponentially. However, most of these empirical relationships were derived under controlled experimental conditions or assuming relatively uniform corrosion. In contrast, corrosion in actual structures is highly non-uniform, influenced by variations in concrete cover thickness and environmental exposure, and commonly develops as a mixed pattern of uniform and localized corrosion. In these cases, fracture behavior is often governed not by the average cross-sectional loss but by stress concentration at the most severely corroded minimum cross-section. Consequently, predictions based solely on mass loss ratio may produce inconsistent results [13–15]. Previous experimental studies considering non-uniform corrosion have also reported that ductility degradation is more strongly governed by localized corrosion features than by averaged corrosion indicators [16,17]. In particular, corrosion morphology and residual cross-sectional characteristics have been shown to significantly influence elongation capacity and fracture behavior of reinforcing bars, even at comparable mass-loss levels [18,19]. These findings suggest that averaged indicators alone may be insufficient to capture the mechanical consequences of non-uniform corrosion.

Nevertheless, obtaining naturally corroded rebars that reflect such localized damage characteristics is inherently challenging. Direct extraction from aging bridge structures is often constrained by practical issues such as traffic control and on-site operational limitations. For this reason, most previous experimental studies have relied on artificially corroded specimens produced using electrochemical acceleration or salt-spray techniques. While such artificial corrosion methods offer efficient control of corrosion levels, they have inherent limitations in reproducing the irregular and non-uniform corrosion characteristics observed in real structures. Consequently, empirical models based on mass loss ratio have primarily been developed under artificial corrosion conditions or relatively uniform corrosion environments, limiting their applicability to naturally corroded rebars subjected to long-term exposure in existing structures.

Most prior studies employed mass loss as a single indicator, the naturally corroded rebars in this study were compared with literature data using the same metric (see Appendix A, Fig. A1). The results showed that, within a similar mass-loss range, the mechanical performance of the naturally corroded specimens exhibited a consistently lower trend than the literature data.

To enhance predictive reliability, this study comparatively analyzed mechanical degradation using multiple indicators and introduced a composite corrosion index that incorporates both pit depth and cross-sectional loss to better represent real corrosion conditions.

2.2.2. Corroded rebar specimen

Most previous experimental studies have employed artificially corroded specimens, in which corrosion was accelerated under controlled laboratory conditions using techniques such as impressed current, salt-spray, or wet–dry cycling [2]. While these methods effectively control the degree of corrosion and shorten testing time, they cannot fully replicate the irregularity and complex interactions characteristic of natural corrosion. In real structures, corrosion develops gradually through the combined effects of chloride diffusion, surface cracking, carbonation, and environmental exposure, resulting in heterogeneous and time-dependent deterioration patterns [6].

Because naturally corroded specimens can only be obtained from aged structures, their availability is inherently limited, resulting in relatively few experimental studies. Nevertheless, several studies have investigated naturally corroded rebars extracted from existing RC structures. For example, Fernández et al. [14] tested rebars extracted from a 30-year-old bridge and reported significant reductions in both strength and elongation. Similarly, Liu et al. [8] and Imperatore [4] found that localized pitting and non-uniform corrosion induce greater variability in tensile strength compared with uniform corrosion assumptions. Recent investigations have shown that the maximum cross-sectional loss ratio correlates more strongly with strength degradation than the average cross-sectional loss ratio [4,8].

Furthermore, recent studies have highlighted the need for realistic datasets that capture spatially distributed corrosion features. Several researchers have also reported that naturally corroded rebars tend to exhibit reduced ductility and brittle failure modes [20,21]. Building upon this background, the present study develops an empirical framework based on field-extracted, naturally corroded rebars to quantitatively link corrosion morphology with mechanical degradation.

3. Materials and methods

3.1. Experimental setup and data acquisition

The investigated rebars were extracted from the cantilever region of the slab of a bridge located on a major traffic network crossing a river in a metropolitan area. According to traffic statistics, the bridge corresponds to a route with very high traffic demand, with an average daily traffic volume of approximately 145,777 vehicles in 2023 and a total of 146,604 vehicles recorded in September 2021. In addition, the bridge deck is exposed to an environment in which chlorides are continuously supplied due to seasonal temperature

variations and repeated deicing operations during winter. According to publicly available data on deicing chemical usage provided by the Seoul Metropolitan Government, the average annual amount of deicing chemicals used on urban expressways in Seoul during recent winter seasons was reported to be approximately 2018 tons, quantitatively supporting that the investigated bridge has been exposed to a long-term chloride environment [22].

The rebars were originally embedded with typical concrete cover thickness for bridge slabs and were not directly exposed prior to corrosion initiation. The specimens were extracted by cutting the deck slab of the target bridge into short segments, followed by concrete crushing. By keeping the cutting length of the slab short, the possibility of bending or residual deformation occurring during lifting and extraction was minimized. After retrieval, no mechanical straightening or surface treatment was performed, and the tensile specimens were prepared with relatively short gauge lengths to reduce the possibility that deformation occurring during the extraction process could affect the mechanical performance measured in the tensile tests. Each tensile specimen had a nominal total length of approximately 250 mm, which is comparable to the effective gauge length commonly adopted in ASTM-based tensile tests for D16 reinforcing bars [23]. All specimens were visually inspected prior to testing, and no cases were observed in which damage originating from the extraction process affected the tensile behavior.

A total of 57 corroded reinforcing bars were extracted from a bridge slab that had been in service for approximately 45 years before replacement due to visible deterioration. Fig. 1 presents representative examples of the extracted specimens, illustrating varying degrees of corrosion ranging from uniform surface rust to severe localized pitting. The average compressive strength of the slab concrete, determined through core testing, was 28.56 MPa. The chloride content measured at the reinforcement depth from the underside of the slab ($\approx$ 40 mm) was approximately 0.004–0.005 % by weight of concrete ($\approx$ 0.10 kg/m^3), indicating a chloride-induced corrosion environment. Based on the corrosion initiation model proposed by Kim [24], corrosion was estimated to have initiated approximately 24.3 years after construction.

After extraction, the rebars were cleaned in accordance with ASTM G1–90 [25] to remove surface corrosion products. The corroded length was defined as the portion of the corroded rebar surface exhibiting visible corrosion, which was measured along the longitudinal axis prior to testing. The mass loss, maximum pit depth, nominal cross-sectional area (D16), and corroded length of each specimen were measured prior to tensile testing, as summarized in Table 2, which presents the pre-test corrosion and geometric parameters of the rebar specimens.

High-resolution video recordings (4 K, 3840 $\times$ 2160 px) were captured for 3D reconstruction following the workflow illustrated in Fig. 2. The reconstruction process comprised sequential frame extraction, point cloud generation, and surface reconstruction, providing a visual overview of the automated 3D modeling procedure. All computational analyses and model reconstructions were performed on a workstation equipped with an Intel Core i7–8700 CPU, 48 GB RAM, and an NVIDIA GeForce RTX 2070 GPU.

3.2. Automated 3D model generation of corroded rebars

Optical methods such as X-ray and 3D scanning—renowned for their non-destructive and high-efficiency evaluation—have been widely applied in civil engineering research [9,26–29]. However, these techniques typically require dedicated infrastructure and are often cost-prohibitive. To overcome these limitations, an automated algorithm was developed in this study to generate 3D models of corroded rebars using low-cost imaging data.

For model reconstruction, video frames were extracted at three frames per second, and distinctive features were identified using the Scale-Invariant Feature Transform algorithm. Image parameters were standardized, with a maximum resolution of 1600 px, a maximum of 6000 features, and a peak threshold of 0.01. Feature correspondences between consecutive frames were obtained through guided matching to minimize errors, followed by geometric refinement using the Difference-of-Gaussian detection and multi-view consistency checks [30].

After feature matching, the 3D geometry of the rebars was reconstructed using the Structure-from-Motion technique, which simultaneously estimates camera parameters and 3D point coordinates based on multi-view projection consistency [31]. The reconstruction accuracy was further refined through bundle adjustment to minimize the total reprojection error:

$$\epsilon = \sum_i ||x_i - \pi(P_i X)||^2$$



Fig. 1. Corroded reinforcing bars extracted from the bridge deck slab.

Table 2
Pre-test corrosion and geometric parameters of rebar specimens.

Specimen ID	Mass Loss (%)	Maximum pit depth (mm)	D16(mm^2)	Corroded Length(mm)
rebar_specimen_1	8.0378	0	198.6	0
rebar_specimen_2	1.6548	0	198.6	0
rebar_specimen_3	8.9835	0	198.6	0
rebar_specimen_4	10.6383	0	198.6	0
rebar_specimen_5	7.8014	0	198.6	0
rebar_specimen_6	8.9835	0	198.6	0
rebar_specimen_7	6.6194	0	198.6	0
rebar_specimen_8	7.0922	0	198.6	0
rebar_specimen_9	0	0	198.6	0
rebar_specimen_10	13.0024	4.2	198.6	31
rebar_specimen_11	8.747	0	198.6	0
rebar_specimen_12	3.7825	0	198.6	0
rebar_specimen_13	13.948	0	198.6	0
rebar_specimen_14	2.6005	1.2	198.6	35
rebar_specimen_15	8.747	3.7	198.6	25.3
rebar_specimen_16	21.2766	3.6	198.6	35
rebar_specimen_17	4.9645	0	198.6	0
rebar_specimen_18	16.5485	3.93	198.6	87
rebar_specimen_19	8.5106	0	198.6	0
rebar_specimen_20	8.5106	0	198.6	0
rebar_specimen_21	12.0567	2.55	198.6	95
rebar_specimen_22	10.4019	1.55	198.6	25.1
rebar_specimen_23	10.8747	1.36	198.6	25.5
rebar_specimen_24	5.4374	0	198.6	0
rebar_specimen_25	8.9835	2.67	198.6	17
rebar_specimen_26	15.8392	4.02	198.6	33
rebar_specimen_27	11.3475	4.8	198.6	23
rebar_specimen_28	13.7116	0	198.6	0
rebar_specimen_29	8.747	6.92	198.6	43
rebar_specimen_30	14.8936	6.9	198.6	30
rebar_specimen_31	18.6761	3.24	198.6	44
rebar_specimen_32	18.4397	8.3	198.6	32
rebar_specimen_33	17.9669	7.17	198.6	34
rebar_specimen_34	22.9314	4.7	198.6	100
rebar_specimen_35	34.7518	8.2	198.6	25
rebar_specimen_36	19.8582	6.6	198.6	15
rebar_specimen_37	13.2388	4.04	198.6	40
rebar_specimen_38	13.7116	9.49	198.6	71
rebar_specimen_39	8.5106	3.38	198.6	10
rebar_specimen_41	31.9149	11.6	198.6	25.5
rebar_specimen_42	24.3499	4.93	198.6	47
rebar_specimen_43	20.0946	5.9	198.6	21
rebar_specimen_44	14.6572	4.02	198.6	55
rebar_specimen_45	26.4775	6.45	198.6	85
rebar_specimen_46	20.5674	5.81	198.6	52
rebar_specimen_47	12.5296	6.43	198.6	44
rebar_specimen_48	16.5485	9.06	198.6	47
rebar_specimen_49	9.4563	5.61	198.6	37
rebar_specimen_50	19.3853	6.86	198.6	70
rebar_specimen_51	12.0567	2.55	198.6	10
rebar_specimen_52	12.0567	8.04	198.6	42
rebar_specimen_53	7.8014	4	198.6	20
rebar_specimen_54	14.1844	6.3	198.6	17
rebar_specimen_55	7.0922	5.09	198.6	20
rebar_specimen_56	17.2577	5.61	198.6	26
rebar_specimen_57	11.8203	5.1	198.6	27
rebar_specimen_61	10.5122	0	198.6	0
rebar_specimen_62	29.8601	10.4	198.6	10.4
rebar_specimen_63	29.8759	8.14	198.6	8.14
rebar_specimen_64	11.8913	3.12	198.6	30
rebar_specimen_65	11.053	2.63	198.6	2.63
rebar_specimen_66	18.588	7.44	198.6	7.44
rebar_specimen_67	24.1194	7.57	198.6	7.57
rebar_specimen_68	11.9819	2.33	198.6	30
rebar_specimen_69	29.6647	9.76	198.6	9.76
rebar_specimen_70	7.525	0	198.6	27.8
rebar_specimen_71	9.20437	6.26	198.6	6.26
rebar_specimen_72	9.03311	0	198.6	0

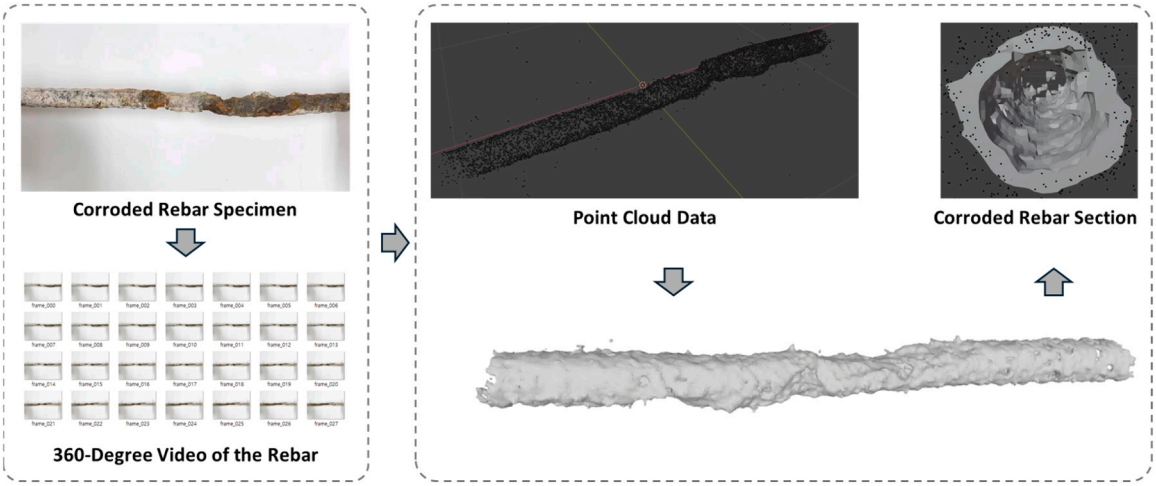

Fig. 2. Workflow for 3D modeling of corroded rebar specimens.

where x_i represents the image coordinate of a 3D point X projected through the camera matrix P_i, and $\pi(\cdot)$ denotes the projection operator. The resulting model was exported in PLY format using the COLMAP converter for subsequent processing.

The generated point cloud initially contained background noise, which was removed through a grid-based (voxel) filtering process.

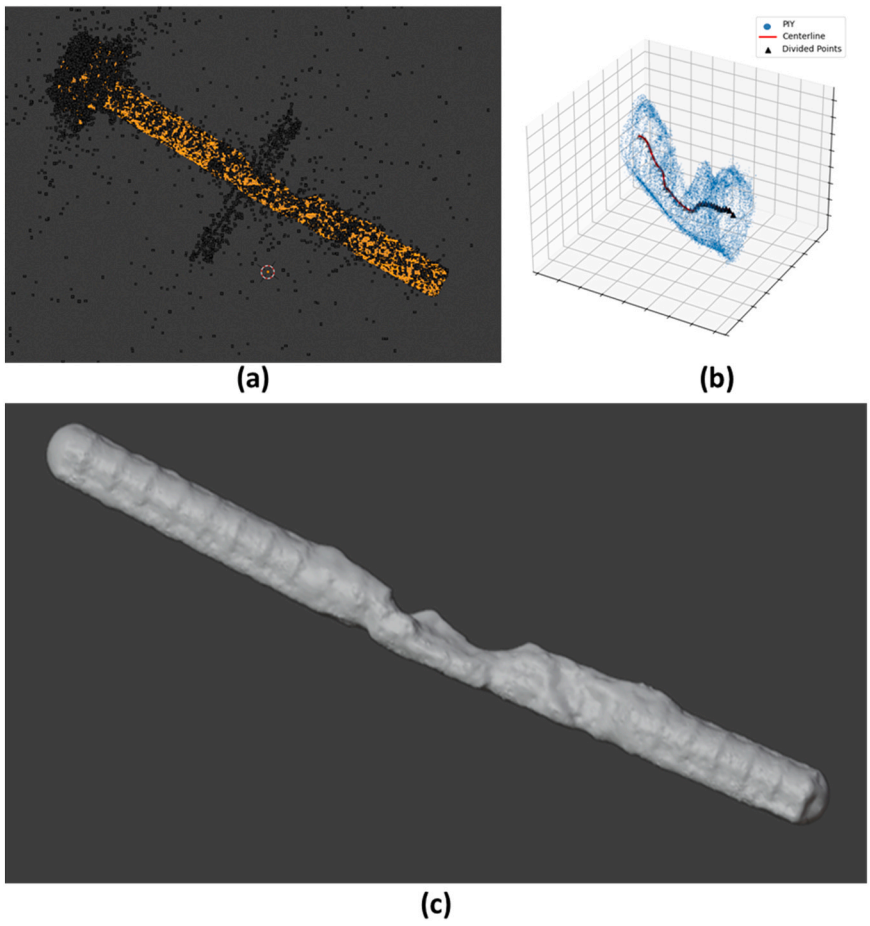

Fig. 3. Summary of 3D reconstruction steps for corroded rebar specimens: (a) denoised point cloud (black: original; orange: filtered), (b) extracted centerline, and (c) reconstructed 3D mesh.

Each point was assigned to a voxel cell based on its spatial coordinates, and voxels containing fewer than a predefined number of points were excluded. The initial filtering parameters were set to a voxel size of 0.008 m and a minimum of five points per voxel. When excessive point loss occurred, the parameters were adaptively adjusted to maintain a balance between denoising and geometric preservation. Consequently, approximately 80 % of the points were retained, effectively preserving the original rebar geometry while suppressing background artifacts. Fig. 3(a) illustrates the denoised point cloud, with the black points representing the original data and the orange points indicating the remaining dataset after noise removal.

To quantify the cross-sectional loss, the reconstructed point cloud of each specimen was sliced along its computed centerline. Although specimens exhibiting excessive curvature were excluded due to the tensile test setup, minor deviations from linearity remained. Therefore, to ensure geometrically consistent cross-sections, slicing planes were defined orthogonal to the local tangent vectors at 100 equally spaced positions along the centerline.

The centerline was established by translating the point cloud $P = \{p_i \in \mathbb{R}^3\}_{i=1}^{N}$ so that its centroid coincided with the origin, followed by singular value decomposition. The first principal component vector, $a = V_1$, was defined as the global axis of the rebar. Each point's axial coordinate was then calculated as

$$t_i = (p_i - C) \bullet a,$$

where C represents the centroid of the point set. The coordinates t_i were uniformly sampled to generate reference positions $\{t_j\}$, and local centroids $c(t_j)$ were computed using Gaussian kernel regression as the weighted mean of neighboring points:

$$c(t_j) = \frac{\sum_i p_i \exp\left[-\frac{1}{2}\left(\frac{t_i - t_j}{h}\right)^2\right]}{\sum_i \exp\left[-\frac{1}{2}\left(\frac{t_i - t_j}{h}\right)^2\right]}$$

where h denotes the kernel bandwidth proportional to the rebar length. Sections where the angle between the global axis a and the local tangent vector $v(t)$ exceeded 20° were excluded to prevent distortion. The resulting centroids were interpolated using a NURBS curve to construct the final centerline geometry for cross-sectional evaluation. The constructed centerline is illustrated in Fig. 3(b), showing the smoothed axial trajectory derived from the denoised point cloud.

The point cloud generated in the previous step consisted of irregularly distributed points, which were converted into a continuous surface for cross-sectional damage analysis. A triangular mesh was reconstructed from the point cloud using the Open3D library [32], as illustrated in Fig. 3(c). To validate the geometric accuracy of the reconstructed model, the rib thickness of the 3D mesh was compared with that of the actual corroded rebar. The deviation, defined as the relative difference between the two measurements, did not exceed 1.2 % for any specimen. This close agreement, shown in Fig. 4, confirms that the reconstructed mesh accurately reproduces the original geometry of the corroded specimens and provides a robust foundation for subsequent cross-sectional evaluation.

Using the reconstructed mesh model, slicing planes were generated orthogonal to the local tangent vectors along the centerline at equally spaced intervals, resulting in 100 cross-sectional planes per specimen. The cross-sectional area at each position was then calculated to assess material loss along the rebar length. The minimum cross-sectional area, corresponding to the most severely corroded region, was identified through this analysis. Fig. 5 presents an example of the cross-sectional evaluation process, showing the variation in residual cross-sectional area along the specimen (left) and the geometric comparison between the reference (non-corroded) and actual corroded sections (right).

3.3. Tensile behavior of corroded reinforcing bars

Tensile tests were conducted under displacement control at a loading rate of 8 mm/min. Specimen slippage during testing can lead

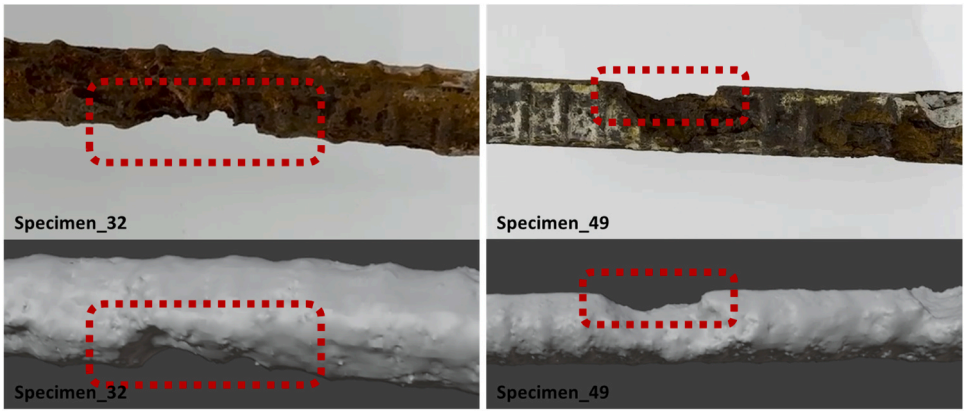

Fig. 4. Comparison between actual corroded rebar specimens and reconstructed 3D mesh models.

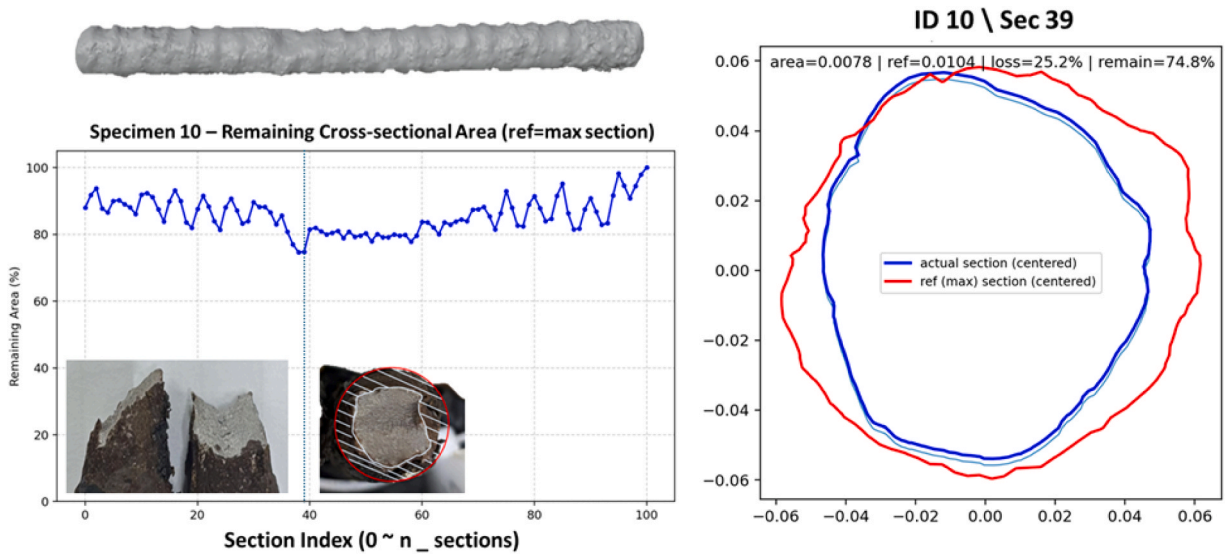

Fig. 5. Cross-sectional evaluation of a corroded rebar specimen: residual cross-sectional area distribution (left) and comparison between reference (red) and corroded (blue) sections (right).

to inaccurate local strain estimation from universal testing machine (UTM) data. To address this issue, a video-based optical tracking method was adopted. The optical-based tracking method was employed as a supplementary tool to qualitatively monitor specimen behavior during testing and to support the assessment of deformation measurement reliability, rather than as a replacement for the displacement data obtained from the testing machine. Each specimen's surface was alternately painted in black and white to enhance contrast, and three pairs of color-coded targets (red, blue, and green) were applied for displacement tracking. The experimental setup and tracking configuration are illustrated in Fig. 6.

In the first frame of each test video, six target regions were segmented using the Segment Anything Model [33], and the centroid

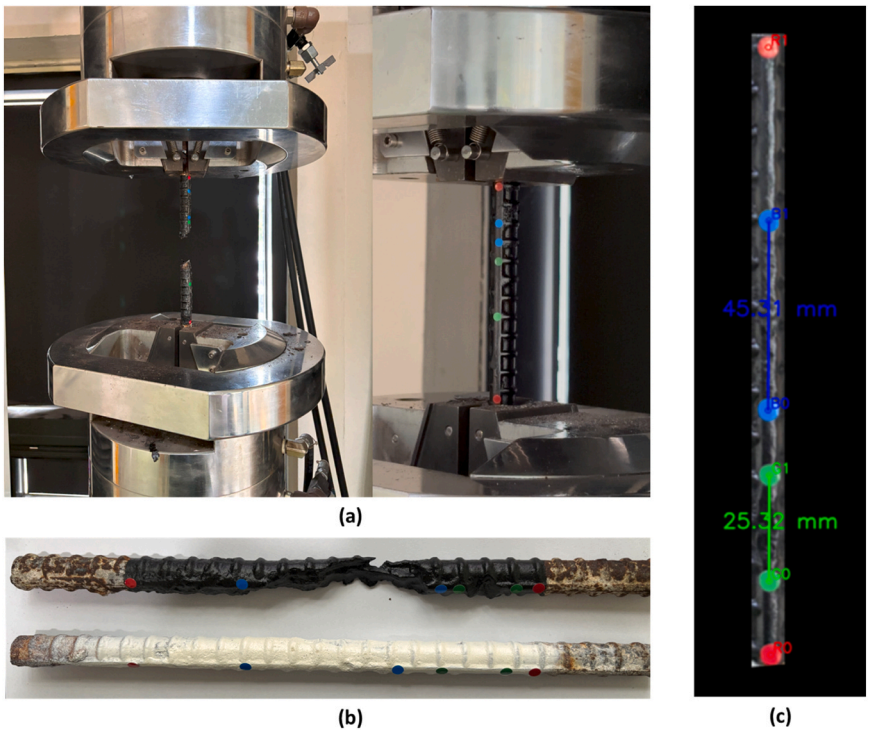

Fig. 6. Experimental setup and optical tracking: (a) tensile testing environment, (b) surface marking with color-coded target points, and (c) target-tracking output.

$\left(x_{c,}\ y_{c,}\right)$ of each segmented region was used as the reference coordinate:

$$\left(x_{c,}\quad y_{c,}\quad\right) = \left(\frac{1}{N}\sum_{i=1}^{N} x_i \quad , \quad \frac{1}{N}\sum_{i=1}^{N} y_i\right)$$

Target displacements between consecutive frames were then tracked using the Kanade–Lucas–Tomasi algorithm [34] under the standard brightness-constancy assumption. For each frame, the distance between paired targets was measured, and a single scale factor—calibrated from the initial gauge length using the red pair—was applied to the blue and green pairs. The validation results, summarized in Table 3, indicate that tracking errors for all specimens remained below 1.6 %, confirming that the optical method achieved sufficient accuracy for local strain evaluation. Specimens for which tracking targets detached during testing were excluded from Table 3, whereas the mechanical performance evaluation was conducted using displacement data obtained from the testing machine.

3.4. Definition of corrosion indicators

The degree of corrosion damage in reinforcing bars is typically quantified using a single indicator, such as the mass loss ratio (ML) or the maximum cross-sectional loss ratio (μ_{max}). However, the mass loss ratio is based on the assumption of uniform corrosion distribution and therefore fails to adequately capture the localized characteristics of corrosion. Several studies have also proposed various individual indicators—such as the cross-sectional loss ratio, maximum pit depth, and corrosion location—but these single parameters remain insufficient to describe the combined effects of corrosion on mechanical degradation.

In this study, the relationships between individual corrosion indicators and the mechanical degradation of corroded rebars were quantitatively evaluated. The reductions in yield and ultimate strengths were modeled as linear, while elongation degradation was represented by an exponential function. Based on these assumptions, correlations between the mechanical degradation ratios and four primary corrosion indicators—mass loss ratio, average cross-sectional loss, maximum pit depth, and residual cross-sectional area ratio—were analyzed. The mass loss ratio and the average cross-sectional loss were adopted to represent averaged corrosion characteristics, whereas the maximum pit depth and the residual cross-sectional area ratio were used to capture the severity of localized corrosion.

All indicators exhibited linear relationships with reductions in yield and ultimate strengths and exponential correlations with decrease in elongation, as illustrated in Fig. 7. The regression analysis results, summarized in Table 4, indicate that the maximum pit depth yielded the highest coefficients of determination (R^2 = 0.827, 0.810, and 0.849, respectively), suggesting that this parameter most reliably explains the mechanical degradation behavior of corroded rebars.

Furthermore, classification of the corroded specimens by corrosion type revealed distinct differences in mechanical degradation. Rebars with pitting corrosion exhibited more pronounced strength and ductility losses than uniformly corroded rebars at comparable single-indicator levels (see Appendix B, Fig. B1).

As shown in Table 4, the average cross-sectional loss (μ) exhibited the lowest coefficient of determination (R^2), whereas the maximum pit depth (Depth/D) showed the highest R^2 value, followed by the residual cross-sectional area ratio (C.R.). The average cross-sectional loss (μ) is calculated by averaging localized corrosion damage along the specimen length and therefore cannot adequately represent the localized pit damage observed in naturally corroded reinforcing bars. Tensile failure of naturally corroded rebars is governed not by the average cross-sectional condition but by stress concentration at the most severely corroded minimum cross-section. Therefore, corrosion indicators based on average cross-sectional loss show lower correlation with mechanical degradation.

To further examine possible nonlinear relationships between corrosion indicators and mechanical degradation parameters, Pearson's correlation coefficient (r), Spearman's rank correlation coefficient (ρ), and mutual information (MI) coefficient were computed, as shown in Fig. 8.

The correlation analysis revealed distinct trends depending on the mechanical property considered. For yield strength, the maximum pit depth exhibited the highest Pearson's r value, indicating that degradation followed a predominantly linear trend. Conversely, the residual cross-sectional area ratio showed a higher Spearman's ρ, suggesting a monotonic yet nonlinear relationship. The MI results further demonstrated a strong dependence on this parameter.

For ultimate strength, most corrosion indicators yielded higher Spearman's ρ values than Pearson's r, implying that monotonic nonlinear correlations were generally more prominent. Both coefficients were notably high for the maximum pit depth, confirming the

Table 3
Statistical summary of target tracking errors used for validation of optical measurement accuracy.

Residual cross sectional area ratio (%)	Mean error [Blue]	Standard deviation [Blue]	Mean error [Green]	Standard deviation [Green]
0–20	0.89	1.23	4.66	6.19
20–40	1.34	1.53	2.07	2.15
40–60	0.78	0.71	1.98	1.63
60–80	2.73	2.50	2.72	2.50
80–100	1.18	1.20	0.91	0.91

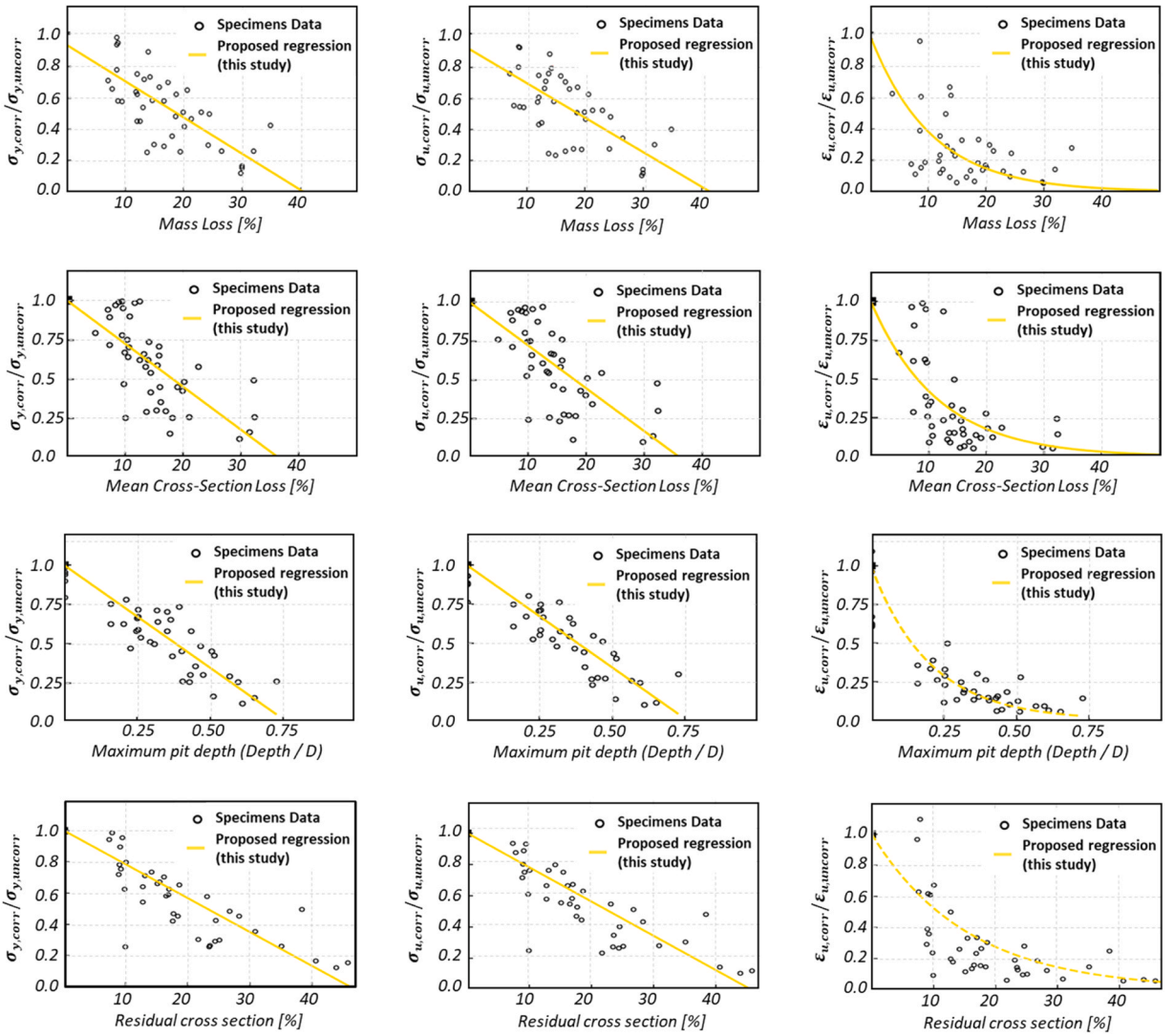

Fig. 7. Relationships between corrosion indicators and mechanical degradation parameters of corroded rebars.

Table 4
Coefficients of determination (R^2) and regression equations for each corrosion indicator.

Corrosion indicator	Yield strength reduction	Ultimate strength reduction	Elongation reduction
Mass Loss (M_{corr})	$R^2 = 0.632$ ($\sigma_{\Delta y} = 1 - 0.0232 \bullet M_{corr}$)	$R^2 = 0.583$ ($\sigma_{\Delta u} = 1 - 0.02227 \bullet M_{corr}$)	$R^2 = 0.579$ $\varepsilon_{\Delta} = e^{-0.09521 M_{corr}}$
Cross-section _mean (μ)	$R^2 = 0.477$ ($\sigma_{\Delta y} = 1 - 0.0274 \bullet \mu$)	$R^2 = 0.462$ ($\sigma_{\Delta u} = 1 - 0.0276 \bullet \mu$)	$R^2 = 0.469$ $\varepsilon_{\Delta} = e^{-0.0859 \mu}$
Maximum pit depth ($Depth/D$)	$R^2 = \mathbf{0.827}$ ($\boldsymbol{\sigma_{\Delta y} = 1 - 1.3078 \bullet (Depth/D)}$)	$R^2 = \mathbf{0.810}$ ($\boldsymbol{\sigma_{\Delta u} = 1 - 1.3112 \bullet (Depth/D)}$)	$R^2 = \mathbf{0.849}$ $\boldsymbol{\varepsilon_{\Delta} = e^{-4.9582 (Depth/D)}}$
Residual cross-sectional area ratio (C.R)	$R^2 = 0.678$ ($\sigma_{\Delta y} = 1 - 0.0108 \bullet C.R$)	$R^2 = 0.689$ ($\sigma_{\Delta u} = 1 - 0.0110 \bullet C.R$)	$R^2 = 0.566$ $\varepsilon_{\Delta} = e^{-0.0324 (C.R)}$

coexistence of linear and nonlinear relationships. Consistently, the MI analysis revealed a high degree of dependency across all indicators.

Regarding elongation, Spearman's ρ exceeded Pearson's r across all indicators, indicating that nonlinear relationships were dominant. The maximum pit depth yielded the highest MI value, demonstrating strong sensitivity to this parameter. Overall, the

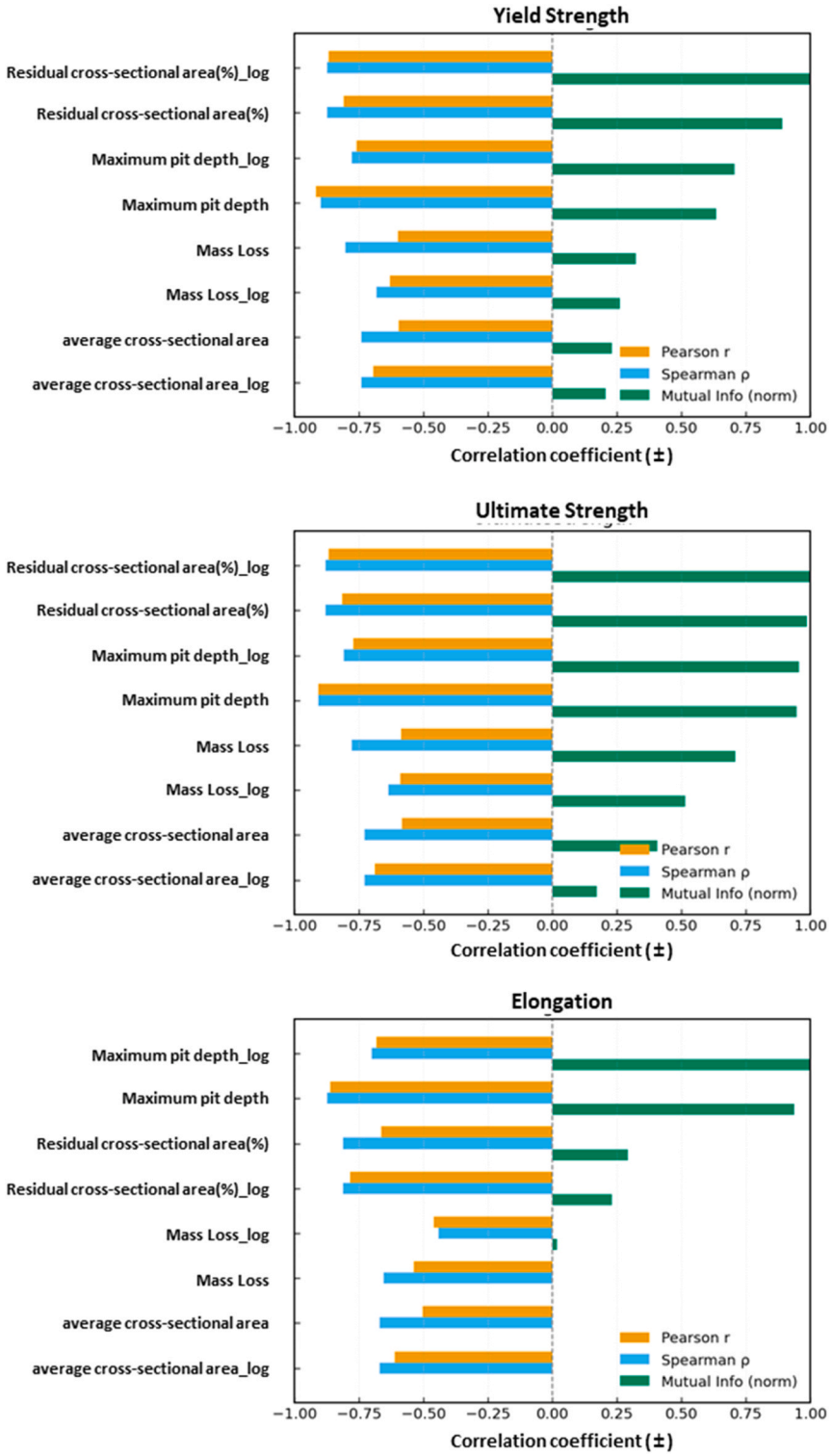

Fig. 8. Comparison of Pearson's r, Spearman's ρ, and mutual information (MI) between corrosion indicators and mechanical degradation parameters: (a) yield strength, (b) ultimate strength, and (c) elongation.

maximum pit depth and the residual cross-sectional area emerged as the most influential indicators governing the mechanical degradation behavior of corroded rebars.

4. Result and discussion

To quantitatively evaluate the mechanical degradation of naturally corroded rebars, regression analyses were performed using both single and composite corrosion indicators. All regressions were conducted using the ordinary least squares (OLS) method, and the weights (w_1, w_2) of the composite indicators were determined through the L-BFGS-B constrained optimization algorithm. The predictive performance of the proposed equations was evaluated through five-fold cross-validation to ensure generalization and stability.

Model performance was assessed using five statistical metrics: the coefficient of determination (R^2), the predictive coefficient of determination (Q^2), the root mean square error (RMSE), the mean absolute error (MAE), and bias. The overall explanatory capability of the developed models was then verified for the degradation ratios of yield strength, ultimate strength, and elongation.

Among the single corrosion indicators, the Depth/D ratio exhibited the strongest correlation with the reduction in yield strength. The regression equation for the single-indicator model is expressed as:

$$(\Delta\sigma_y = \mathbf{1} - \mathbf{1.3078} \bullet (\boldsymbol{Depth/D})) \quad , \quad \boldsymbol{R^2} = \mathbf{0.827}, \quad \boldsymbol{Bias} = \mathbf{0.018}, \quad \boldsymbol{MAE} = \mathbf{0.090}$$

When the residual cross-sectional area ratio (C.R) is included as an auxiliary variable, the composite model becomes:

$$(\Delta\sigma_y = 1 - (1.2328 \bullet \left(0.75 \bullet \frac{Depth}{D}\right) + (0.25 \bullet C.R)) \quad , \quad \boldsymbol{R^2} = \mathbf{0.867}, \quad \boldsymbol{Bias} = \mathbf{0.001}, \quad \boldsymbol{MAE} = \mathbf{0.081}$$

In the left image of Fig. 9, yellow points denote observations expressed by the single indicator Depth/D, with the yellow line depicting its OLS fit. The same observations mapped to the composite indicator appear as blue points, with the blue line showing the corresponding fit. The right image of Fig. 9 presents a comparison of the two models using R^2, Q^2, RMSE, Bias, and MAE.

Compared with the single-indicator model, the composite indicator increases R^2 from 0.827 to 0.867 and enhances Q^2, while RMSE, Bias, and MAE all decrease, indicating smaller and less directional errors. Taken together, the shift from yellow to blue in the left panel and the corresponding metrics in the right panel show that the composite indicator provides a more accurate and reliable representation of yield-strength degradation in naturally corroded rebars.

Following the analysis of yield strength degradation, the degradation behavior of ultimate strength was examined. In this case, the Depth/D ratio again emerged as the most influential single corrosion indicator. The regression relationship can be expressed as:

$$(\Delta\sigma_{ult} = \mathbf{1} - \mathbf{1.3112} \bullet (\boldsymbol{Depth/D})) \quad , \quad \boldsymbol{R^2} = \mathbf{0.810}, \quad \boldsymbol{Bias} = \mathbf{0.019}, \quad \boldsymbol{MAE} = \mathbf{0.095}$$

When the residual cross-sectional area ratio (C.R.) is incorporated as a secondary variable, the composite regression becomes:

$$(\Delta\sigma_{ult} = 1 - (1.2328 \bullet \left(0.75 \bullet \frac{Depth}{D}\right) + (0.25 \bullet C.R)) \quad , \quad \boldsymbol{R^2} = \mathbf{0.857}, \quad \boldsymbol{Bias} = \mathbf{0.000}, \quad \boldsymbol{MAE} = \mathbf{0.082}$$

As shown in Fig. 10, the composite model demonstrates a visibly improved fit, with the data points shifting closer to the regression line and the overall scatter reduced. The statistical metrics, presented on the right, corroborate this improvement: R^2 increased from 0.810 to 0.857 and Q^2 also improved, while RMSE, Bias, and MAE all decreased. Collectively, these results indicate that the composite indicator provides a more accurate and consistent representation of ultimate-strength degradation in naturally corroded rebars.

In contrast to strength-related properties, the degradation of elongation exhibited a markedly nonlinear pattern, which was best captured by an exponential decay relationship with the Depth/D ratio:

$$(\Delta\varepsilon_{max} = \boldsymbol{exp}(-\mathbf{4.9582} \bullet (\boldsymbol{Depth/D})) \quad , \quad \boldsymbol{R^2} = \mathbf{0.849}, \quad \boldsymbol{Bias} = \mathbf{0.022}, \quad \boldsymbol{MAE} = \mathbf{0.089}$$

The relationship was best described by the exponential function:

$$(\Delta\varepsilon_{max} = \boldsymbol{exp}(-\mathbf{4.6991} \bullet \left(0.855 \bullet \frac{Depth}{D}\right) + (0.145 \bullet C.R)) \quad , \quad \boldsymbol{R^2} = \mathbf{0.882}, \quad \boldsymbol{Bias} = \mathbf{0.009}, \quad \boldsymbol{MAE} = \mathbf{0.089}$$

As shown in Fig. 11, the composite model exhibits a slightly improved fit, with reduced scatter observed in the lower elongation range. Although the MAE remained constant at 0.089, both R^2 and Q^2 increased, and RMSE and Bias decreased, indicating greater stability and reduced directional error. These results suggest that incorporating the residual cross-sectional area enhances the model's ability to capture the nonlinear effects of corrosion on ductility, providing a more consistent representation of elongation degradation across the full corrosion range.

Mass loss and average cross-sectional area can be considered as additional candidates for composite indicators; however, they were excluded from the final composite formulation in this study. This decision was made because the mechanical degradation of corroded reinforcing bars is more closely associated with stress concentration induced by localized corrosion rather than with averaged section loss. As shown in the correlation analysis in Fig. 8, mass loss and average cross-sectional area exhibited relatively lower correlation with mechanical degradation compared to indicators reflecting localized corrosion characteristics. Therefore, the composite indicator in this study was constructed using the maximum pit depth and the residual cross-sectional area ratio (C.R.), which directly represent the effects of localized corrosion.

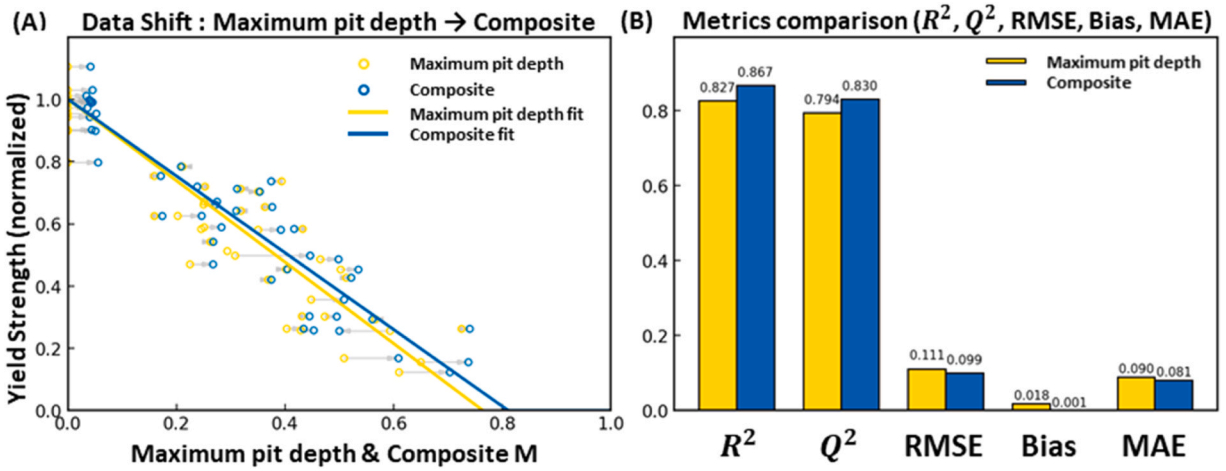

Fig. 9. Comparison between single and composite indicator models for yield strength degradation.

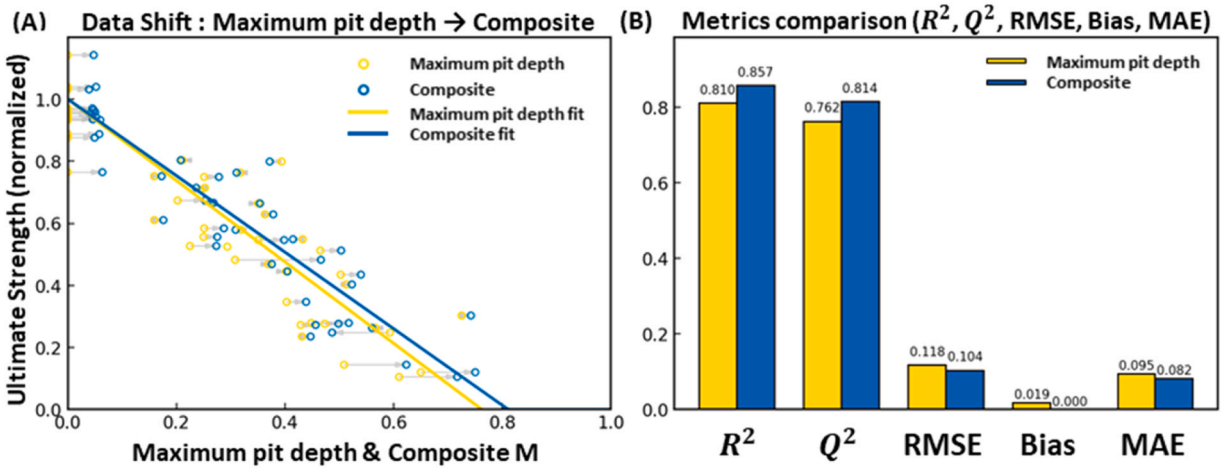

Fig. 10. Comparison between single and composite indicator models for ultimate strength degradation.

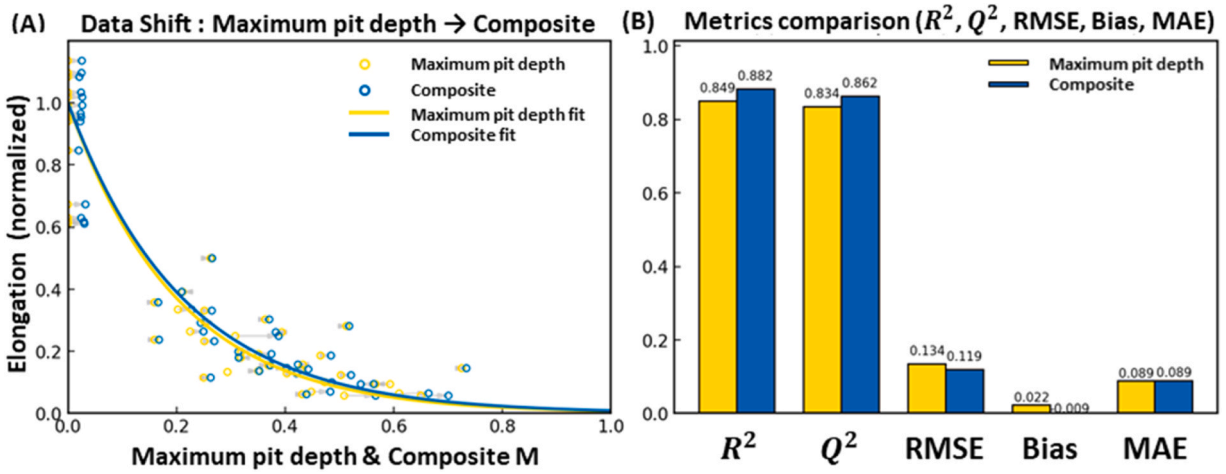

Fig. 11. Comparison between single and composite indicator models for elongation degradation.

5. Conclusion

In this study, the relationship between cross-sectional corrosion characteristics and the mechanical degradation of naturally corroded reinforcing bars was quantitatively evaluated. The analysis utilized specimens extracted from a 45-year-old bridge, where corrosion was estimated to have initiated approximately 24.3 years after construction. A composite corrosion indicator was formulated by combining the maximum pit depth and the residual cross-sectional area ratio for mechanical degradation were derived.

The main findings of this study are summarized as follows:

(i) The composite-indicator models demonstrated higher explanatory capability and smaller prediction errors (RMSE, Bias, and MAE) than the single-indicator models, providing a more consistent representation of the degradation behavior of yield strength, ultimate strength, and elongation. This improved performance is attributed to the use of the residual cross-sectional area ratio, defined at the minimum cross-section at the fracture location, together with the maximum pit depth, which effectively capture the non-uniform corrosion characteristics of naturally corroded reinforcing bars.

(ii) The proposed composite-indicator equations allow a simple yet rational estimation of the residual mechanical performance of corroded rebars and can serve as practical input parameters for durability evaluation and corrosion-integrated analytical models of deteriorated RC structures.

(iii) The experimental dataset encompassed specimens with corrosion mass-loss ratios ranging from 0 % to approximately 35 %, corresponding to residual cross-sectional area ratios of 0.7–1.0 and maximum pit-depth ratios up to $\approx$ 0.7.Accordingly, the proposed empirical relationships are applicable within this experimental range, and their validity beyond these limits requires further verification.

From a practical bridge-deck maintenance perspective, corrosion of reinforcing bars often occurs in the upper reinforcement layers, where chloride ingress and moisture accumulation are severe. During repair or rehabilitation works, the removal of deteriorated cover concrete exposes the corroded rebars, providing a critical opportunity to directly inspect their corrosion condition and evaluate their residual mechanical performance. In this context, the composite corrosion indicator and degradation models proposed in this study can be applied to assess the residual tensile strength and ductility of exposed rebars, thereby supporting performance-based maintenance planning and remaining service-life assessment of aging reinforced concrete bridge decks.

Overall, the proposed models for the reduction in yield strength, ultimate tensile strength, and elongation of corroded steel reinforcement provide a practical basis for evaluating the residual load-carrying capacity and ductility of reinforced concrete structures containing corroded rebars.

CRediT authorship contribution statement

Shim Changsu: Writing – review & editing, Validation, Supervision, Resources, Project administration, Funding acquisition, Conceptualization. **Jihun Shin:** Writing – original draft, Methodology, Investigation, Data curation.

Declaration of Competing Interest

The authors declare that they have no known competing financial interests or personal relationships that could have appeared to influence the work reported in this paper.

Acknowledgements

This research was conducted with the support of the “National R&D Project for Smart Construction Technology (RS-2020-KA156007)” funded by the Korea Agency for Infrastructure Technology Advancement under the Ministry of Land, Infrastructure and Transport, and managed by the Korea Expressway Corporation.

Appendix

A. Comparison with literature data

This appendix compares the mechanical performance of the naturally corroded rebars tested in this study with published datasets that used mass loss as the corrosion indicator. As shown in Fig. A1, within a comparable mass-loss range of 10–30 %, the specimens in this study consistently exhibited lower normalized strength and elongation than those reported in the literature. This difference is attributed to the influence of localized pitting corrosion and the minimum cross-sectional area, suggesting that mass loss alone may not adequately capture the actual mechanical degradation of naturally corroded rebars.

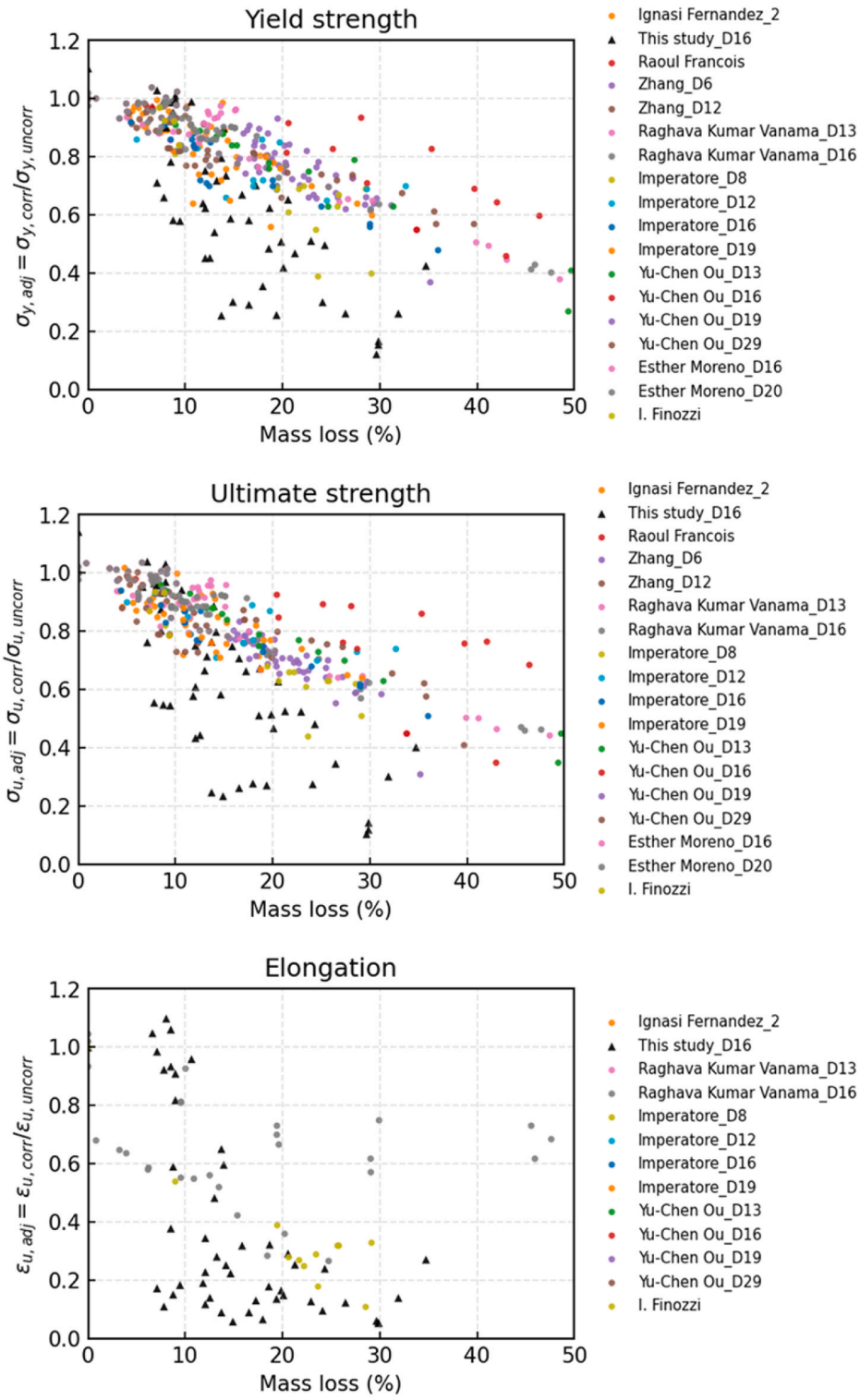

Fig. A1. Normalized strength and elongation according to mass loss (10–30 %) for specimens from the present study and reported literature

B. Effect of corrosion type on mechanical degradation under different indicators

This appendix presents a detailed analysis of the mechanical degradation of naturally corroded rebars based on their corrosion morphology. As shown in Fig. B1, classifying the specimens by corrosion type revealed distinct mechanical response patterns between

uniformly and locally corroded rebars. Specifically, pitted rebars (black markers) exhibited more pronounced reductions in strength and ductility than uniformly corroded rebars (blue markers) at comparable single-indicator levels.

These results indicate that localized corrosion exerts a stronger influence on mechanical degradation, supporting the higher explanatory capability of the maximum pit depth relative to the mass-loss-based indicator.

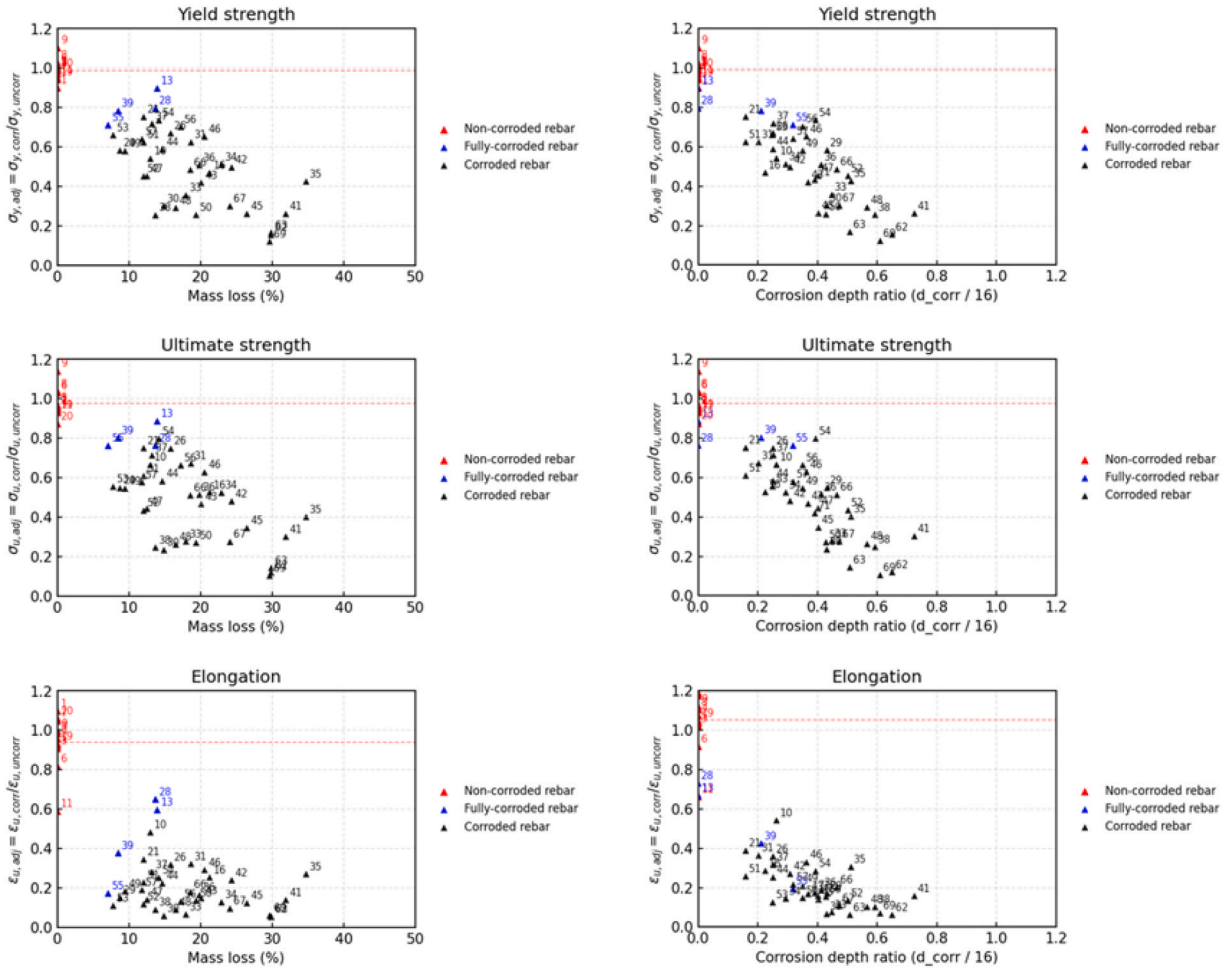

Fig. B1. Comparison of mechanical degradation by corrosion type under different indicators

Data availability

Data will be made available on request.

References

[1] K. Tuutti, Corrosion of Steel in Concrete, Swedish Cement and Concrete Research Institute, Stockholm, 1982.
[2] C. Alonso, C. Andrade, J. Rodríguez, J.M. Diez, Factors controlling cracking of concrete affected by reinforcement corrosion, Mater. Struct. 31 (1998) 435–441, https://doi.org/10.1007/BF02480466.
[3] S. Imperatore, Z. Rinaldi, C. Drago, Degradation relationships for the mechanical properties of corroded steel rebars, Constr. Build. Mater. 148 (2017) 219–230, https://doi.org/10.1016/j.conbuildmat.2017.04.209.
[4] S. Imperatore, Mechanical properties decay of corroded reinforcement in concrete—an overview, Infrastructures 7 (12) (2022) 170, https://doi.org/10.3390/infrastructures7120170.
[5] E. Moreno, A. Cobo, G. Palomo, M.N. González, Mathematical models to predict the mechanical behavior of reinforcements depending on their degree of corrosion and the diameter of the rebars, Constr. Build. Mater. 61 (2014) 156–163, https://doi.org/10.1016/j.conbuildmat.2014.03.003.
[6] Y.-C. Ou, Y.T.T. Susanto, H. Roh, Tensile behavior of naturally and artificially corroded steel bars, Constr. Build. Mater. 103 (2016) 93–104, https://doi.org/10.1016/j.conbuildmat.2015.10.075.
[7] C.H. Jeon, J.B. Lee, S. Lon, C.S. Shim, Mechanical behavior of corroded prestressing steel strands based on corrosion morphology, J. Mater. Res. Technol. 8 (2) (2019) 2450–2460, https://doi.org/10.1016/j.jmrt.2019.04.018.

[8] X. Liu, Y. Chen, J. Li, Y. Zhao, Degradation of steel rebar tensile properties affected by longitudinal non-uniform corrosion, Materials 16 (7) (2023) 2917, https://doi.org/10.3390/ma16072917.
[9] G. Wang, Y. Ma, L. Wang, J. Zhang, Experimental study and residual fatigue life assessment of corroded high-tensile steel wires using 3D scanning technology, Eng. Fail. Anal. 124 (2021) 105335, https://doi.org/10.1016/j.engfailanal.2021.105335.
[10] Hansco Co., Ltd, 2024. SD300 Rebar mechanical properties. Hansco Official Website. Available at: ⟨https://www.hansco.co.kr⟩ (accessed 3 November 2025).
[11] B.C. Hwang, S.J. Kim, J.H. Lee, Manufacturing and technological trends of high-strength reinforcing bars for seismic resistance, Korean J. Met. Mater. 54 (12) (2016) 862–874, https://doi.org/10.3365/KJMM.2016.54.12.862.
[12] G. Ahmed, M.A. Al-Eshaikh, A.S. Al-Najmi, Degradation mechanisms and residual mechanical properties of corroded reinforcing steel bars, Constr. Build. Mater. 338 (2022) 127601, https://doi.org/10.1016/j.conbuildmat.2022.127601.
[13] R. François, I. Khan, V.H. Dang, Impact of corrosion on mechanical properties of steel embedded in 27-year-old corroded reinforced concrete beams, Mater. Struct. 46 (2013) 899–910, https://doi.org/10.1617/s11527-012-9941-z.
[14] I. Fernández, J.M. Bairán, A.R. Marí, Corrosion effects on the mechanical properties of reinforcing steel bars: Fatigue and σ–ε behavior, Constr. Build. Mater. 101 (2015) 772–783, https://doi.org/10.1016/j.conbuildmat.2015.10.139.
[15] W. Zhang, X. Song, X. Gu, S. Li, Tensile and fatigue behavior of corroded rebars, Constr. Build. Mater. 34 (2012) 409–417, https://doi.org/10.1016/j.conbuildmat.2012.02.071.
[16] W. Zhu, R. François, C.S. Poon, J.G. Dai, Influences of corrosion degree and corrosion morphology on the ductility of steel reinforcement, Constr. Build. Mater. 148 (2017) 297–306, https://doi.org/10.1016/j.conbuildmat.2017.05.079.
[17] C.A. Apostolopoulos, V.G. Papadakis, Consequences of steel corrosion on the ductility properties of reinforcement bar, Constr. Build. Mater. 22 (12) (2008) 2316–2324, https://doi.org/10.1016/j.conbuildmat.2008.01.006.
[18] W. Zhu, R. François, Effect of corrosion pattern on the ductility of tensile reinforcement extracted from a 26-year-old corroded beam, Adv. Conc. Constr. 1 (2) (2013) 121–136, https://doi.org/10.12989/acc.2013.1.2.121.
[19] J. Liu, X. Luo, Q. Chen, Degradation of steel rebar tensile properties affected by longitudinal non-uniform corrosion, Materials 16 (7) (2023) 2917, https://doi.org/10.3390/ma16072917.
[20] I. Fernández, C.G. Berrocal, Mechanical properties of 30-year-old naturally corroded steel reinforcing bars, Int. J. Concr. Struct. Mater. 13 (2019) 9, https://doi.org/10.1186/s40069-018-0308-x.
[21] J. Miao, Y. Li, C. Wang, T. Zhang, A practical approach to determining mechanical degradation of corroded rebar, Constr. Build. Mater. 429 (2025) 142284, https://doi.org/10.1016/j.conbuildmat.2025.142284.
[22] Seoul Metropolitan Government, 2025. Annual deicing chemical usage on urban expressways in Seoul [dataset]. Public Data Portal. ⟨https://www.data.go.kr/data/15129601/fileData.do?recommendDataYn=Y⟩ (Accessed 15 May 2025).
[23] J.H. Lee, D.H. Kim, J.H. Choi, Evaluation of minimum extensibility standard requirements for steel reinforcement, J. Korea Concr. Inst. 23 (5) (2011) 559–567.
[24] K. Kim, Empirical data-driven digital twin for predicting service life of bridge slabs under chloride exposure. [Master's thesis], Chung-Ang University, Seoul, Republic of Korea, 2025.
[25] ASTM International, ASTM G1-90: Standard Practice for Preparing, Cleaning, and Evaluating Corrosion Test Specimens, ASTM International, West Conshohocken, PA, USA, 2011.
[26] M.M. Kashani, A.J. Crewe, N.A. Alexander, Use of a 3D optical measurement technique for stochastic corrosion pattern analysis of reinforcing bars subjected to accelerated corrosion, Corros. Sci. 73 (2013) 208–221, https://doi.org/10.1016/j.corsci.2013.03.009.
[27] S. Lim, M. Akiyama, D.M. Frangopol, Assessment of the structural performance of corrosion-affected RC members based on experimental study and probabilistic modeling, Eng. Struct. 127 (2016) 189–205, https://doi.org/10.1016/j.engstruct.2016.08.040.
[28] M. Tahershamsi, I. Fernández, K. Lundgren, K. Zandi, Investigating correlations between crack width, corrosion level and anchorage capacity, Struct. Infrastruct. Eng. 13 (10) (2017) 1294–1307, https://doi.org/10.1080/15732479.2016.1263673.
[29] M. Zhang, H. Song, S. Lim, M. Akiyama, D.M. Frangopol, Reliability estimation of corroded RC structures based on spatial variability using experimental evidence, probabilistic analysis and finite element method, Eng. Struct. 192 (2019) 30–52, https://doi.org/10.1016/j.engstruct.2019.04.001.
[30] D.G. Lowe, Distinctive image features from scale-invariant keypoints, Int. J. Comput. Vis. 60 (2) (2004) 91–110, https://doi.org/10.1023/B:VISI.0000029664.99615.94.
[31] J.L. Schönberger, J.M. Frahm, Structure-from-motion revisited. Proceedings of the IEEE Conference on Computer Vision and Pattern Recognition (CVPR), 2016, pp. 4104–4113, 10.1109/CVPR.2016.445.
[32] Zhou, Q.-Y., Park, J., Koltun, V., 2018. Open3D: A Modern Library for 3D Data Processing. arXiv:1801.09847.
[33] Kirillov, A., Mintun, E., Ravi, N., Mao, H., Rolland, C., Gustafson, L., Xiao, T., Whitehead, S., Berg, A.C., Lo, W.Y., Dollár, P., Girshick, R., 2023. Segment Anything. arXiv preprint arXiv:2304.02643. ⟨https://arxiv.org/abs/2304.02643⟩.
[34] J.Y. Bouguet, Pyramidal Implementation of the Lucas–Kanade Feature Tracker: Description of the Algorithm, Intel Corporation, Microprocessor Research Labs, 2001. Technical Report.